Published in final edited form as:
Ultrasound Med Biol. 2015 March ; 41(3): 685–697. doi:10.1016/j.ultrasmedbio.2014.09.016.

Noninvasive In Vivo Characterization of Human Carotid Plaques with Acoustic Radiation Force Impulse (ARFI) Ultrasound: Comparison with Histology Following Endarterectomy

Tomasz J. Czernuszewicz[1], **Jonathon W. Homeister**[2,3], **Melissa C. Caughey**[4], **Mark A. Farber**[5], **Joseph J. Fulton**[5], **Peter F. Ford**[5], **William A. Marston**[5], **Raghuveer Vallabhaneni**[5], **Timothy C. Nichols**[2,4], and **Caterina M. Gallippi**[1,3,6,7,*]

[1]Joint Department of Biomedical Engineering, University of North Carolina and North Carolina State University, Chapel Hill, NC, USA

[2]Department of Pathology and Laboratory Medicine, University of North Carolina, Chapel Hill, NC, USA

[3]McAllister Heart Institute, University of North Carolina, Chapel Hill, NC, USA

[4]Department of Medicine, University of North Carolina, Chapel Hill, NC, USA

[5]Department of Surgery, University of North Carolina, Chapel Hill, NC, USA

[6]Department of Electrical and Computer Engineering, North Carolina State University, Raleigh, NC, USA

[7]Biomedical Research Imaging Center, University of North Carolina, Chapel Hill, NC, USA

Abstract

Ischemic stroke from thromboembolic sources is linked to carotid artery atherosclerotic disease with a trend toward medical management in asymptomatic patients. Extent of disease is currently diagnosed by noninvasive imaging techniques that measure luminal stenosis, but it has been suggested that a better biomarker for determining risk of future thromboembolic events is plaque morphology and composition. Specifically, plaques that are composed of mechanically-soft lipid/necrotic regions covered by thin fibrous caps are the most vulnerable to rupture. An ultrasound technique that noninvasively interrogates the mechanical properties of soft tissue, called acoustic radiation force impulse (ARFI) imaging, has been developed as a new modality for atherosclerotic plaque characterization using phantoms and atherosclerotic pigs, but the technique has yet to be validated *in vivo* in humans. In this preliminary study, *in vivo* ARFI imaging is presented in a case-study format from four patients undergoing clinically-indicated carotid endarterectomy and compared to histology. In two type Va plaques, characterized by lipid/necrotic cores covered by

*Corresponding author: cmgallip@bme.unc.edu, Phone: (919) 843-6647, Address: 152 MacNider Bldg. CB #7575, Chapel Hill, NC 27599, USA.

fibrous caps, mean ARFI displacements in focal regions were high relative to the surrounding plaque material, suggesting soft features covered by stiffer layers within the plaques. In two type Vb plaques, characterized by heavy calcification, mean ARFI peak displacements were low relative to the surrounding plaque and arterial wall, suggesting stiff tissue. This pilot study demonstrates the feasibility and challenges of transcutaneous ARFI for characterizing the material and structural composition of carotid atherosclerotic plaques via mechanical properties, in humans, *in vivo*.

Keywords

atherosclerosis; stroke; plaque characterization; carotid endarterectomy; CEA; acoustic radiation force; ARFI; ultrasound

Introduction

Stroke is one of the leading causes of death and long-term disability in the United States (Go et al., 2013). It is estimated that 87% of all strokes are related to ischemia secondary to atherosclerotic disease (Go et al., 2013) with 15-20% attributable to plaques located in the carotid arteries (Mughal et al., 2011). Degree of carotid stenosis is a standard metric in the evaluation of cerebrovascular risk and, as of today, is one of the most valued parameters used to guide the course of medical treatment in the clinic (Brott et al., 2011). In asymptomatic patients with high grade stenosis, it has been shown that prophylactic carotid endarterectomy (CEA) can reduce the absolute risk of stroke by ∼5% as compared to medical management (Halliday et al., 2010). Based on these numbers though, 20 patients must undergo CEA to prevent one stroke, and potential non-stroke complications in CEA patients such as myocardial infarction or cranial nerve injury could reduce quality of life. Some have even questioned the applicability of these data to today's patients given the significant improvements in pharmaceutical therapies, e.g. statins, anti-hypertensives, etc., and reduction in smoking rates (Abbott, 2009; Selim and Molina, 2011). Current estimates suggest that only 5% of patients with asymptomatic carotid stenosis will benefit from prophylactic CEA (Selim and Molina, 2011). Therefore, there is a great need for an improved method of predicting which patients are at high risk for stroke to enhance the benefit and cost-efficacy of CEA (as well as other interventions).

Many have argued that plaque vulnerability based on plaque structure and composition is a more appropriate biomarker, compared to luminal stenosis, for predicting future thromboembolic events (Moreno, 2010). Vulnerable plaque has been studied extensively in the coronary arteries (Finn et al., 2010). For carotid arteries, the literature is somewhat sparser, but it has been shown that the same general compositional elements correlate with plaque instability, i.e. thin fibrous cap, large lipid/necrotic core, and dense macrophage infiltrate (Redgrave et al., 2006). Although the mechanisms are not completely understood and may include destabilizing effects of matrix metalloproteinases (Newby et al., 2009) and endothelial cell apoptosis (Chan et al., 2013), it is thought that at least one of the reasons these compositional elements confer a higher risk for rupture is that the softer plaque components (e.g. lipids, inflammation, etc.) significantly increase the local circumferential

stress experienced by the fibrous cap (Cardoso and Weinbaum, 2013). When local stresses exceed the ultimate stress (i.e. maximum stress at failure), plaque rupture occurs, and an ischemic event is likely to follow. The "critical" fibrous-cap thickness in carotid plaques, based on CEA specimens, has been reported as a minimum thickness of <200 μm and a representative/average thickness of <500 μm, which is higher than the <65 μm critical thickness reported in coronaries (Redgrave et al., 2008).

Based on the significant amount of literature on the morphological and biomechanical mechanisms that confer plaque rupture risk, many groups in the medical imaging community have attempted to develop noninvasive modalities that can reliably characterize atherosclerotic lesions (for a background on invasive plaque characterization imaging modalities, the reader is referred to the reviews by Jaguszewski et al. (2013), Garcia-Garcia et al. (2011), and Ben-Dor et al. (2011)). X-ray computed tomography (CT) has shown excellent sensitivity to calcium deposition, but only moderate accuracy for lipid cores and hemorrhage (Wintermark et al., 2008). Magnetic resonance imaging (MRI) has been shown to have higher sensitivities to soft-tissue components including lipid cores, fibrosis, hemorrhage, and thrombosis (Cai et al., 2002; Moody et al., 2003; Watanabe et al., 2008). Though the initial data from these modalities look promising, the high monetary cost, ionizing radiation in the case of CT, and specialized surface coils necessary in the case of MRI make widespread implementation challenging and may preclude the use of these modalities for screening.

As an alternative to the more expensive noninvasive modalities, a number of groups have proposed to characterize plaque composition with transcutaneous ultrasound. Plaques that appear echolucent on B-mode have been shown to contain higher amounts of lipid and soft tissue whereas plaques that appear echogenic are generally composed of fibrotic or calcified tissue (Grønholdt et al., 1997, 2002; Kardoulas et al., 1996). In a recent review by ten Kate et al. (2010) though, the authors showed large variability in the reported sensitivities and specificities and concluded that, as of today, B-mode ultrasound alone is too inconsistent and is of limited value compared to MRI or CT when it comes to plaque characterization.

A relatively new approach to characterizing material properties of arteries with ultrasound has been the use of elasticity imaging. Unlike conventional B-mode ultrasound, which generates images of the *acoustic* properties of tissue, elasticity imaging generates images of the *mechanical* properties of tissue. Typically, these methods work by measuring a strain that is the result of either an intrinsic (e.g. cardiac pulsation) or extrinsic (e.g. acoustic radiation force) stress. Examples of noninvasive ultrasonic arterial elasticity imaging that use intrinsic tissue motion include noninvasive vascular elastography (Naim et al., 2013) and pulse wave imaging (Vappou et al., 2010), whereas examples of radiation force techniques include supersonic shear imaging (Couade et al., 2010), lamb-wave dispersion ultrasound vibrometry (Bernal et al., 2011), vibroacoustography (Pislaru et al., 2008), and acoustic radiation force impulse (ARFI) imaging (Nightingale et al., 2002). In ARFI, which is the focus of this current work, radiation-force impulses are generated by a commercially-available ultrasound scanner to focally displace tissue (on the order of 1-10 μm). The resulting displacements in the region of excitation (ROE) are monitored with correlation-based motion tracking methods and used to qualitatively infer tissue stiffness, which

indicates plaque composition. Although the numbers vary widely in the literature, studies on the mechanical properties of atherosclerotic plaques have shown significant differences in the radial Young's modulus of various plaque components suggesting applicability of elasticity imaging; in Lee et al. (1992) calcified tissue was shown to be significantly stiffer (∼354 kPa) than non-fibrous (∼41 kPa) or fibrous tissue (∼81 kPa), whereas lipid/necrotic tissue has been estimated to be the softest component (∼1 kPa) by other groups (Ohayon et al., 2008; Williamson et al., 2003).

The literature supporting the use of ARFI for plaque characterization has been growing rapidly. Work has been done in arterial-mimicking inclusion phantoms (Dumont et al., 2009), finite element method (FEM) models (Doherty et al., 2012), porcine arteries both *ex vivo* (Behler et al., 2013; Dumont et al., 2006) and *in vivo* (Behler et al., 2009), human popliteal and femoral arteries both *ex vivo* (Trahey et al., 2004) and *in vivo* (Dumont et al., 2009), and human carotids *in vivo* (Allen et al., 2011; Dahl et al., 2009). These studies suggest that lipid/necrotic cores tend to displace further than normal arterial tissue, whereas fibrotic or calcified tissue tend to displace less than normal arterial tissue. Although ARFI has begun to be translated to *in vivo* settings in humans, these preliminary experiments were not performed with radiological or histological validation. The goal of this study is to compare ARFI images of human carotid plaques taken *in vivo* to CEA specimens characterized histologically and test the hypothesis that ARFI can be used to characterize human carotid plaque, *in vivo*.

Methods

Patients

Data sets were obtained from eight patients scheduled for CEA in an on-going clinical study (ClinicalTrials.gov number, NCT01581385) at the University of North Carolina (UNC) at Chapel Hill. Selected subjects either had symptomatic carotid artery disease with a stenosis or lesion in the carotid artery thought to be the source of emboli, or asymptomatic carotid artery disease with a >60% internal carotid artery (ICA) stenosis. Carotid duplex ultrasounds were performed by the IAC-accredited UNC Peripheral Vascular Lab (PVL) as part of the patients' standard medical care. The degree of stenosis was determined with an internally validated velocity profile criteria (Table 1). Subjects were considered symptomatic if they had a history of amaurosis fugax, transient ischemic attack (TIA), or minor (non-disabling) stroke referable to the carotid artery distribution. Institutional review board (IRB) approval was obtained for both the patient consent forms and the study protocol, and informed consent was obtained from each study participant. A comprehensive list of patient characteristics is given in Table 2.

Ultrasonic Imaging and Data processing

Investigative B-mode and ARFI imaging were performed with a Siemens Acuson Antares imaging system (Siemens Medical Solutions USA, Ultrasound Division), equipped with the Axius Direct Ultrasound Research Interface (URI) that allowed customizable beam sequencing and access to the raw radiofrequency (RF) data, and a VF7-3 linear array transducer. ARFI ensembles consisted of two reference pulses, one acoustic radiation force

(ARF) excitation pulse, and 60 tracking lines with an 11.5 kHz pulse repetition frequency (PRF). ARFI excitations were 300 cycles (~71 μsec) at 4.21 MHz with a scanner output power of 55%, and both tracking and reference lines were two cycles at 6.15 MHz. The focal configuration, or f-number (F/#, defined as the ratio of focal depth, *z*, to aperture width, *d*), of the excitation pulse was set to 1.5. The reference/tracking pulses used an F/1.5 configuration on transmit and dynamic focusing and aperture growth on receive (F/0.75). The focus in elevation, set by a cylindrical lens, was 3.8 cm. The ARFI beam sequence acquired 40 ensembles spaced 0.35 mm apart, generating an effective lateral field of view (FOV) of 1.4 cm. ARF ensembles were acquired using wiperblading, a scanning mode that acquired lines in a non-serial order across the lateral FOV to minimize heating and reduce interference between consecutive ARF excitations. A single ensemble was captured from the far left of the FOV, then the center, then one position to the right of the far left, then one position right of center, etc., such that no two consecutive ensembles were captured in two adjacent lateral locations. One spatially-matched B-mode frame (220 A-lines, 0.18 mm spacing) preceded each two-dimensional (2D) ARFI acquisition for anatomical reference. The $MI_{.3}$ of the ARFI sequences employed in this study was 1.81, measured at a focal depth of 2 cm that was representative of the imaging depths investigated in this study. The $I_{SPTA.3}$ was measured to be 1.67 W/cm^2. Acoustic intensity measurements were made using an Onda HGL-0200 hydrophone (Onda Corp., Sunnyvale, CA) in a water tank (21 °C) and the phantom-substitution technique described in Palmeri et al. (2005). Heating associated with ARFI sequences was estimated (neglecting perfusion and other cooling effects) to be below 1°C in tissue (Palmeri and Nightingale, 2004; Palmeri et al., 2005).

Images were acquired the day of surgery prior to patient sedation by a registered sonographer trained in ARFI and peripheral vascular imaging. The carotid bifurcation and ICA were imaged longitudinally, using electrocardiogram (ECG) gating to capture sequences during diastole. The ARFI imaging focal depth was chosen based on the location of the plaque, which in all cases in this study was the distal (relative to the transducer) arterial wall. Two repeated acquisitions were acquired in case of scanner failure or unexpected patient motion. The number of repeated acquisitions was limited to two in order to reduce the time of patient imaging and prevent delays to the surgical staff. Raw RF data was saved to the hard drive of the scanner and transferred to a computer for offline post-processing using custom software implemented in MATLAB (Mathworks Inc., Natick, MA). Of the repeated acquisitions, the one included for analysis was chosen subjectively for best image quality based on the authors' experience evaluating arterial ARFI images.

Axial displacements induced by ARF were measured using one-dimensional normalized cross correlation applied to the RF data ensembles as described by Pinton et al. (2006). Specific parameters of the motion tracking algorithm included; 4× spline-based upsampling of RF data (natively sampled at 40 MHz), 376-μm kernel length (i.e. 1.5λ, where λ is the wavelength of the tracking pulse assuming a speed of sound of 1540 m/s), and an 80-μm search region. Motion tracking error for this imaging configuration based on the Cramér-Rao Lower Bound was estimated to be 0.7 μm, assuming 53% fractional bandwidth, 0.999 correlation coefficient, and 40 dB SNR (Walker and Trahey, 1995). Linear motion filtering was applied to the displacement profiles to reduce artifacts introduced by physiological

motion (Fahey et al., 2007; Nightingale et al., 2002). From the acquired ARFI data, 2D parametric images of peak ARFI-induced displacement (PD) were generated. For analysis, ARFI images were overlaid on top of spatially-matched B-mode images with transparency in order to better visualize anatomical structure. B-mode images were generated from raw RF data, and were calculated as the log compressed, absolute value of the Hilbert-transformed RF data. Interpretation of ARFI images was performed by a single reader not blinded to the histological images.

Histology

After CEA specimens were extracted *en bloc*, the vascular surgeon placed a colored suture to indicate specimen orientation (proximal vs. distal relative to the heart), and specimens were photographed and immediately transferred to 10% neutral-buffered formalin for a minimum of 48 hours. Once fixed, the specimens were cut with a scalpel into two halves following the surgeon's anterior/longitudinal arteriotomy. The arteriotomy was assumed to approximately follow the ultrasound imaging plane as both ultrasound and the surgical approach followed an anterior trajectory to avoid the sternocleidomastoid muscle. In all samples obtained in this study, the surgical arteriotomy extended through the length of the sample and was easily identifiable without extra marking. To preserve sample orientation in histological slides, sutures were removed and replaced with tissue marking dyes (Polysciences Inc., Warrington, PA) that would remain on the exterior of the sample after histological staining. After mark-up, gross microscopic images were taken of the luminal face of each sample for reference with a Leica MZ9.5 dissecting microscope (Leica Microsystems GmbH, Wetzlar, Germany) at 6.3× magnification, and samples were embedded in paraffin. An example of sample preparation is depicted in Figure 1.

The samples were sectioned (5-μm slice thickness) and stained with hematoxylin and eosin (H&E), Von Kossa (VK) for calcium, and either Lillie's modified Masson's trichrome (LMT) or a combined Masson's elastin (CME) stain for collagen and elastin fibers. A more detailed guide to histological stains is given in Table 3. De-calcification was not performed on any of the samples in order to preserve calcium for histological staining. For samples with heavy calcification, paraffin blocks were left to soak for 3 days in water to achieve usable sections. Approximately 1 mm of tissue was sectioned from each half of the specimen using a serial-interrupted protocol where 6 serial sections were taken (to allow multiple stains), followed by a 100 μm skip, and another 6 serial sections, etc. Slides containing the stained sections were digitized using a ScanScope digital-slide scanner (Aperio Technologies Inc., Vista, CA) at 20× magnification. The slides that qualitatively matched the plaque morphology from B-mode were chosen, and a blinded pathologist with experience in atherosclerosis examined and annotated the digitized slides using ImageScope (Aperio Technologies Inc., Vista, CA), a freely-available slide viewing/annotation software package. The following features, if present, were identified: fibrous cap/tissue, lipid/necrotic core, calcium, foam cells, vascularity, intra-plaque hemorrhage, and surface thrombus. As was done in Redgrave et al. (2008), lipid/necrotic core was defined as amorphous material containing cholesterol crystals, intra-plaque hemorrhage was defined as an area of erythrocytes within the plaque causing disruption of the plaque architecture, and surface thrombus defined as an organized collection of fibrin and erythrocytes in the lumen. Plaques

were then assigned a rating using the American Heart Association (AHA) classification scale (Table 4) (Stary, 2000). Alignment between ARFI images and histological sections was achieved by manually identifying unique features in both ARFI and histology images (i.e. large calcium deposits or plaque morphological features such as the plaque shoulder).

Results

Carotid plaques were imaged without adverse event from five males and three females immediately prior to undergoing CEA. Data from four patients was excluded for various reasons; in two patients the extracted sample was damaged/lost during surgery, in a third patient, ARFI imaging was incorrectly focused on a portion of arterial wall rather than plaque, and in a fourth patient the ARFI image could not be successfully matched to histology due to lack of common morphology. Patient characteristics and labeling scheme for included patients are presented in Table 2. Matched B-mode and ARFI ultrasound images are presented with corresponding histological sections in Figure 2 through Figure 5. All images (both ultrasonic and histologic) are oriented such that the cephalad portion (i.e. towards the patient's head) of the artery is always on the left side of the image.

Figure 2 shows the imaging results from a symptomatic 57 year-old male (Patient “A”) with a past medical history of hypertension, hyperlipidemia, non-insulin dependent diabetes mellitus, and smoking (quit ∼13 years). Indications for surgery included paresthesia (left face) and previous TIA. Duplex ultrasound revealed significant stenosis in the left CCA and ICA (it was noted that velocities may be underestimated in the ICA due to CCA occlusion). CEA was performed on both CCA and ICA, and results are shown for the CCA. B-mode imaging shows a generally echolucent plaque (Figure 2a), with two echogenic foci located at lateral positions 1.8 mm and 11.6 mm. ARFI imaging (Figure 2b) shows that the plaque exhibits generally low displacement throughout except for a focal, higher-displacing region located towards the right part of the plaque. A low-displacing region separating a high-displacing region from lumen has previously been shown to be indicative of fibrous cap (Behler et al., 2009). A magnification of the ARFI image is provided in Figure 2c, with the higher-displacing region outlined in yellow (mean PD: 3.11 ± 3.6 μm), the echogenic regions outlined in magenta (mean PD: 1.18 ± 0.4 μm), and the plaque outlined in white (mean PD excluding yellow and magenta regions: 1.25 ± 0.7 μm). Histological staining (Figure 2d, e, f) shows a type Va plaque with a necrotic core (Figure 2f, yellow outline) covered by a fibrous cap (Figure 2f, black arrows). Two calcium deposits are also apparent (Figure 2f, magenta arrows) on the bottom center and bottom right of the specimen separated by ∼10 mm. A magnification of the necrotic core located above the left-most calcium deposit is displayed in the inset panel (Figure 2f.1) showing cholesterol clefts and extravascular erythrocytes, indicating mild intra-plaque hemorrhage.

Figure 3 shows the imaging results from a 53 year-old symptomatic female (Patient “B”) with a past medical history of hypertension, hyperlipidemia, diabetes mellitus, smoking, peripheral vascular disease, and claudication. Records note that the patient previously experienced right-sided facial droop, some right arm weakness, and symptoms consistent with amaurosis fugax (specifically, unable to see out of right eye for a few minutes). B-mode imaging shows a plaque in the distal wall with a number of small echogenic foci

scattered throughout, suggesting small calcium deposits (Figure 3a, white arrows), and a focal stenosis extending ~4 mm into the lumen (Figure 3a, asterisk). ARFI imaging (Figure 3b), focused at a depth of 2.6 cm, shows that the plaque exhibits generally low displacement throughout except for a higher-displacing region located underneath the shoulder of the plaque, suggesting fibrous cap. A magnified version of the ARFI image is depicted in Figure 3c, with the higher-displacing region outlined in yellow (mean PD: 2.77 ± 1.7 μm), the echogenic regions outline in magenta (mean PD: 0.85 ± 0.3 μm), and the plaque outlined in white (mean PD excluding yellow and magenta regions: 1.35 ± 0.8 μm). Histological staining (Figure 3d, e, f) shows a type Va plaque with a cellular region with inflammation and early necrotic-core formation (Figure 3f, yellow outline) covered by a fibrous cap (Figure 3f, black arrows). Small, sub-millimeter calcifications are also apparent (Figure 3e, magenta arrow). Figure 3f.1 and Figure 3f.2 show magnified versions of the necrotic/inflamed region and fibrous-cap regions, respectively.

Figure 4 shows a highly occlusive plaque located in the bifurcation of an asymptomatic 72 year-old male (Patient “C”) with a history of hyperlipidemia, hypertension, and smoking. Duplex imaging studies measured a Class 4 stenosis with peak systolic and diastolic velocities of 458 cm/sec and 138 cm/sec, respectively, in the proximal portion of the right ICA. B-mode imaging shows a very complicated and obstructed lumen (Figure 4a) with large shadowing artifact (Figure 4a, white arrows) in the distal wall, suggesting heavy calcification. In this imaging plane, the proximal wall is not clearly defined and tissue appears to extend from the proximal wall to make contact with the calcification in the distal wall. In the ARFI image (Figure 4b), focused at a depth of 2.3 cm, there is a large displacement contrast between plaque in the distal wall (Figure 4b, asterisk) and the tissue that connects to the proximal wall (Figure 4b, dagger). Figure 4c shows a magnification of the ARFI image with the distal plaque outlined in solid white line (mean PD: 2.1 ± 1.5 μm). Mean PD of the tissue connecting to the proximal wall was measured to be 6.0 ± 3.4 μm. Histological staining shows a type Vb plaque with a large calcium deposit indicated by black stain outline (Figure 4d, asterisk), measuring approximately 7.9 mm laterally and 4.5 mm axially, located in the arterial wall distal to the transducer. The tissue extending from the calcification and connecting up to the proximal wall is comprised of collagen fibers (Figure 4d.1 and Figure 4e.1). As seen in the higher-magnification images, the collagen fibers appear loosely-packed and disorganized and do not follow the longitudinal histology plane, suggesting that this tissue may be from the split in the bifurcation. Note that the disruptions in continuity of tissue surrounding the calcium deposit are artifacts of histological processing and are not indicative of plaque rupture.

Figure 5 shows a calcified plaque from a 65 year-old male (Patient “D”) with a history of asymptomatic carotid artery stenosis. Previous cerebral angiogram of this patient demonstrated a 70% stenosis in the left ICA, and was corroborated by duplex scanning which measured peak systolic and diastolic velocities of 455 cm/sec and 143 cm/sec, respectively. B-mode imaging (Figure 5a) shows slight shadowing (Figure 5a, white arrows) below plaque located in the distal wall. In the ARFI image (Figure 5b), focused at a depth of 2.0 cm, the portion of the plaque encroaching into the lumen appears to consist primarily of low-displacing tissue except for a small high-displacing region located toward the bottom of the plaque, which could suggest a fibrous cap. Mean PDs in the plaque (excluding the high-

displacing area) were measured to be 1.85 ± 1.0 μm (Figure 5c, white outline) and 8.27 ± 12.5 μm in the high displacing area (Figure 5c, yellow outline). Large amounts of calcium deposition in this sample can be observed in the gross microscopic image of this sample (Figure 5d, dashed black outline), and confirmed by dark staining on H&E and VK (Figure 5e, f) making this a type Vb plaque. In the CME stain (Figure 5g), there is evidence of degraded collagen surrounding parts of the calcification (Figure 5g.1, black arrow).

Discussion

This work represents a preliminary study of ARFI imaging for characterizing carotid plaque composition in patients undergoing CEA. From the patients that were imaged, a range of atherosclerotic lesions were observed during histological analysis including plaques with heavy calcium deposition, loose and dense fibrosis, necrotic cores containing crystallized cholesterol, and mild intra-plaque hemorrhage. Agreeing with previous animal and *ex vivo* studies (Behler et al., 2013, 2009; Dumont et al., 2006; Trahey et al., 2004), ARFI imaging showed regions of contrast that were consistent with underlying compositional elements determined from histology.

In this study, large lipid/necrotic core, dense inflammation, and/or intra-plaque hemorrhage was seen on histology in two of the four CEA specimens (patients A and B). ARFI images of plaques containing these features were characterized by an identifiable area of increased peak displacement (∼3× greater) below an area of lower displacement that has previously been shown to indicate a soft necrotic core covered by a stiff fibrous cap (Behler et al., 2009). Indeed, in patient A, the plaque was composed of a large necrotic region (as seen by the cholesterol clefts left on histology) covered by a fibrous cap, and in patient B, the plaque had a cellular region of inflammation and early necrotic core surrounded by a large amount of fibrosis. By measuring the thickness of the low-displacing region separating the high-displacing region from the lumen, ARFI imaging may be able to estimate fibrous cap thickness, another potential indicator of plaque vulnerability (Redgrave et al., 2008), however this analysis was outside the scope of this manuscript.

The other two examples presented in this work included predominately calcified plaques. In general, ARFI displacements were low, which could be expected of a stiff calcification, but, relatively higher ARFI displacements were also observed. In patient C, higher-displacing tissue was seen to extend up to the proximal wall from the calcification in the distal wall, and in patient D, a focal region of high displacement was noted in the bottom of the plaque (having a similar signature to patients A and B). In both of these cases, histology indicated that tissue surrounding the calcification was partially composed of loose/degraded collagen deposition, which could explain the higher displacements observed in these regions. The magnitude of displacements though, in these regions, was similar or greater to those seen in plaques with necrotic core, which would be expected to be mechanically softer than collagen. Likewise, the magnitude of displacements in the calcified regions of these plaques was similar to regions of dense collagen in the type Va examples, despite calcium being the stiffest plaque component (Lee et al., 1992). One explanation for these confounding results may be that the applied force was not constant across the area of the plaque due to boundary conditions and/or variations in the absorption coefficient of plaque components. For

example, calcium in particular has been shown to be highly absorbing (Shi et al., 2009), which could increase the magnitude of radiation force for a given acoustic intensity level. If the calcium deposit experiences more force, it may displace just as far as mechanically-softer, less-absorbing tissue despite inherently having a higher Young's modulus value. Conversely, depending on the magnitude of attenuation, some parts of the plaque could experience less radiation force due to the exponential decay in acoustic intensity of the ARF pulse through depth. An example of this can be seen in patient D (Figure 5b, white arrows); the soft tissue underneath the calcification appears to displace less than the surrounding, but this is most likely an artifact of unequal force distribution rather than a true contrast in tissue stiffness. These results suggest that ARFI measurements of displacement need to be interpreted with care and should be evaluated qualitatively taking boundary conditions and absorption into account.

There are a number of other factors that could influence the appearance of plaques in ARFI images. First, mechanical-wave propagation away from the ROE can affect both apparent lesion size and contrast (Nightingale et al., 2006; Palmeri et al., 2006). Typically, these effects are seen later in the ARFI imaging time-course and would not be expected to significantly alter a measurement of peak displacement, which is usually computed from the early time samples. To test this, we examined the median time-to-peak values for patients A and B, and found that a majority of the peak displacements occurred within 0.26 or 0.35 ms after the ARF excitation, suggesting minimal impact of mechanical-wave propagation on the PD images. Second, boundary artifacts of the cross-correlation method could affect the resolution of the ARFI images and impact low-displacing feature size measurements. The resolution of ARFI, like conventional compressive elastography, is comparable to the B-mode resolution and is dictated by both ultrasound parameters (frequency, bandwidth, etc.) and signal-processing parameters (kernel size and kernel step) (Nightingale, 2011; Pinton et al., 2006; Righetti et al., 2002). Pinton et al. (2006) examined the impact of kernel size on estimation of a step displacement and showed that as the kernel size increased, the slope of the measured step response decreased, effectively reducing the contrast of the ‘edge’. For our ARFI images, a kernel size of 1.5λ was utilized suggesting features of ∼400 μm axially could be detected given sufficient mechanical contrast. As has been hypothesized previously (Allen et al., 2011), it is possible that as the size of a plaque feature, such as fibrous cap, decreases, the feature will move in unison with underlying softer features, such as necrotic cores, making it difficult to resolve on an ARFI image even if the feature thickness exceeds axial resolution limits of the system. Despite this limitation, ARFI imaging may be able to infer the presence of a thin fibrous cap by virtue of the proximity of a high-displacing region to the lumen.

A significant challenge in this study was ensuring spatial alignment between the ultrasonic and histologic imaging planes. In order to accomplish this, the following general regions had to be identified on the specimen: cephalad vs. thoracic and distal vs. proximal (in relation to the transducer). Identifying distal vs. proximal wall was the more difficult task and relied on the assumption that the anterior arteriotomy made by the surgeon approximated the ultrasonic imaging plane. This assumption was based on the fact that the position of the patient during imaging and surgery was consistent (patient was in a supine position with head tilted away ∼45 degrees from midline), and both imaging and surgery followed a

trajectory just anterior to the sternocleidomastoid muscle. Although care was taken to ensure alignment, it was possible that the surgical cut did not exactly follow the ultrasonic imaging plane. Specifically, three degrees of freedom (translation in elevational dimension, rotation around lateral dimension, and rotation around axial dimension) could not be precisely controlled. Complicating alignment even further was the fact that histological specimens were both unpressurized and fixed, which could have caused significant changes in tissue size (Dalager-Pedersen et al., 1999). In order to overcome the limitations of alignment inherent in CEA histological validation, comparison between ARFI and other *in vivo* plaque characterization technologies, such as MRI, may be required, although aligning MRI and ARFI imaging planes could also pose significant challenges.

While these results are encouraging, there are a number of steps necessary to continue the development of ARFI for plaque characterization. First, given the small sample size of this pilot study, ARFI-derived plaque composition could not be statistically correlated with patients' symptoms. Much larger clinical end-point studies will need to be performed to confirm that ARFI-derived elastograms are relevant to predicting ischemic event. Second, atherosclerotic lesions imaged in this study were significantly advanced (all patients were Class 4 on the UNC Doppler-indicated stenosis scale) and may not be representative of earlier stage plaques. Prior non-validated studies in humans though (Dahl et al., 2009), have shown that ARFI is capable of revealing areas of mechanical contrast similar to those seen in this study, suggesting that the technique may be relevant in plaques not indicated for surgery by Doppler. Third, ARFI beam sequences were designed conservatively; the number of ARFI interrogations was kept to a maximum of 40, consequently limiting the imaging FOV to ∼1.5 cm, and the output power of the scanner was kept relatively low (55% of total output). Under this regime, the full lateral extent of the plaque was not imaged in some cases, and the induced displacements sometimes challenged the limits of the displacement tracking algorithm, which was estimated to be ∼0.7 μm. In the future, more interrogation points along the lateral dimension could be acquired such that the full lateral extent of the plaque would be covered. Also, increasing the radiation force amplitude could improve the contrast and signal-to-noise ratio (SNR) of the images particularly for stiff plaque features where displacements were seen to fall below 1 μm.

Finally, it is important to consider the safety of using ARFI for plaque characterization especially when the plaque is vulnerable to rupture. Displacing a vulnerable plaque with ARF is considered safe due to the low mechanical pressure applied by the excitation. In an FEM study, Doherty et al. (2013) investigated stress distributions of ARFI excitations on vulnerable carotid plaques. It was found that the peak von Mises stress experienced by a thin fibrous cap overlaying a large lipid core was significantly less (by two orders of magnitude) than the circumferential stress induced by blood pulsation as well as the widely-cited ultimate stress of plaque rupture (300 kPa). Although these data regarding the safety of ARFI plaque imaging are relevant throughout the cardiac cycle, we chose a conservative approach and employed ECG gating to trigger the ARFI excitation pulses during diastole. During diastole, inherent blood pressure on the plaque is at its lowest in the cardiac cycle, and thus the cumulative ARFI- and blood flow-induced stress on the plaque will be lowest.

Conclusion

ARFI imaging was applied successfully in a small number of patients undergoing clinically-indicated CEA. With matched histology, it was shown that plaques composed of lipid/necrotic core, mild intra-plaque hemorrhage, inflammation, and loose/degraded collagen deposition had focal regions of relatively high peak displacements. On the contrary, plaques composed of dense collagen deposition and/or calcium were generally low-displacing. Overall, these results represent the first comparison of histology and *in vivo* ARFI imaging of carotid plaque. Identification of plaque mechanical properties with ARFI could substantially improve plaque vulnerability assessment ultimately leading to better patient risk stratification not only in asymptomatic patients with high-grade stenosis, but also in patients with <60% occlusion where Doppler ultrasound may be less reliable (Gough, 2011; Wasserman et al., 2005). In future work, ARFI sensitivity and specificity for characterizing atherosclerotic features will be quantified with receiver operating characteristic (ROC) curve analysis.

Acknowledgments

We thank Siemens Medical Solutions USA, Inc. Ultrasound Division for technical support. We also gratefully acknowledge M.W. Fisher for help with patient recruitment and consent, B. J. Q. Nichols for help with sample collection, K. McNaughton and J. A. Ezzell of the UNC Histology Research Core Facility, and the residents and staff of UNC Vascular Surgery.

Financial Support: This work was supported by NIH grants R01HL092944, K02HL105659, and T32HL069768, and the UNC Glaxo Foundation Fellowship.

References

Allen JD, Ham KL, Dumont DM, Sileshi B, Trahey GE, Dahl JJ. The development and potential of acoustic radiation force impulse (ARFI) imaging for carotid artery plaque characterization. Vasc Med. 2011; 16:302–311. [PubMed: 21447606]

Behler RH, Czernuszewicz TJ, Wu C, Nichols TC, Zhu H, Homeister JW, Merricks EP, Gallippi CM. Acoustic Radiation Force Beam Sequence Performance for Detection and Material Characterization of Atherosclerotic Plaques: Preclinical, Ex Vivo Results. IEEE Trans Ultrason Ferroelectr Freq Control. 2013 In Press.

Behler RH, Nichols TC, Zhu H, Merricks EP, Gallippi CM. ARFI imaging for noninvasive material characterization of atherosclerosis Part II: Toward in vivo characterization. Ultrasound Med Biol. 2009; 35:278–295. [PubMed: 19026483]

Ben-Dor I, Mahmoudi M, Pichard AD, Satler LF, Waksman R. Optical coherence tomography: a new imaging modality for plaque characterization and stent implantation. J Interv Cardiol. 2011; 24:184–92. [PubMed: 21198851]

Bernal M, Nenadic I, Urban MW, Greenleaf JF. Material property estimation for tubes and arteries using ultrasound radiation force and analysis of propagating modes. J Acoust Soc Am. 2011; 129:1344–1354. [PubMed: 21428498]

Brott TG, Halperin JL, Abbara S, Bacharach JM, Barr JD, Bush RL, Cates CU, Creager Ma, Fowler SB, Friday G, Hertzberg VS, McIff EB, Moore WS, Panagos PD, Riles TS, Rosenwasser RH, Taylor AJ. 2011 ASA/ACCF/AHA/AANN/AANS/ACR/ASNR/CNS/SAIP/SCAI/SIR/SNIS/SVM/SVS guideline on the management of patients with extracranial carotid and vertebral artery disease: executive summary: a report of the American College of Cardiology Foundation/American Heart. J Am Coll Cardiol. 2011; 57:1002–44. [PubMed: 21288680]

Cai JM, Hatsukami TS, Ferguson MS, Small R, Polissar NL, Yuan C. Classification of human carotid atherosclerotic lesions with in vivo multicontrast magnetic resonance imaging. Circulation. 2002; 106:1368–1373. [PubMed: 12221054]

Cardoso L, Weinbaum S. Changing Views of the Biomechanics of Vulnerable Plaque Rupture: A Review. Ann Biomed Eng. 2013

Chan HC, Ke LY, Chu CS, Lee AS, Shen MY, Cruz Ma, Hsu JF, Cheng KH, Chan HCB, Lu J, Lai WT, Sawamura T, Sheu SH, Yen JH, Chen CH. Highly electronegative LDL from patients with ST-elevation myocardial infarction triggers platelet activation and aggregation. Blood. 2013

Couade M, Pernot M, Prada C, Messas E, Emmerich J, Bruneval P, Criton A, Fink M, Tanter M. Quantitative assessment of arterial wall biomechanical properties using shear wave imaging. Ultrasound Med Biol. 2010

Dahl JJ, Dumont DM, Allen JD, Miller EM, Trahey GE. Acoustic radiation force impulse imaging for noninvasive characterization of carotid artery atherosclerotic plaques: a feasibility study. Ultrasound Med Biol. 2009; 35:707–716. [PubMed: 19243877]

Doherty JR, Dumont DM, Trahey GE, Palmeri ML. Acoustic radiation force impulse imaging of vulnerable plaques: a finite element method parametric analysis. J Biomech. 2012

Dumont D, Behler RH, Nichols TC, Merricks EP, Gallippi CM. ARFI imaging for noninvasive material characterization of atherosclerosis. Ultrasound Med Biol. 2006; 32:1703–1711. [PubMed: 17112956]

Dumont D, Dahl JJ, Miller E, Allen J, Fahey B, Trahey GE. Lower-limb vascular imaging with acoustic radiation force elastography: demonstration of in vivo feasibility. IEEE Trans Ultrason Ferroelectr Freq Control. 2009; 56:931–944. [PubMed: 19473912]

Fahey BJ, Palmeri ML, Trahey GE. The impact of physiological motion on tissue tracking during radiation force imaging. Ultrasound Med Biol. 2007; 33:1149–1166. [PubMed: 17451869]

Finn AV, Nakano M, Narula J, Kolodgie FD, Virmani R. Concept of vulnerable/unstable plaque. Arter Thromb Vasc Biol. 2010; 30:1282–1292.

Garcia-Garcia HM, Gogas BD, Serruys PW, Bruining N. IVUS-based imaging modalities for tissue characterization: similarities and differences. Int J Cardiovasc Imaging. 2011; 27:215–224. [PubMed: 21327914]

Go AS, Mozaffarian D, Roger VL, Benjamin EJ, Berry JD, Borden WB, Bravata DM, Dai S, Ford ES, Fox CS, Franco S, Fullerton HJ, Gillespie C, Hailpern SM, Heit Ja, Howard VJ, Huffman MD, Kissela BM, Kittner SJ, Lackland DT, Lichtman JH, Lisabeth LD, Magid D, Marcus GM, Marelli A, Matchar DB, McGuire DK, Mohler ER, Moy CS, Mussolino ME, Nichol G, Paynter NP, Schreiner PJ, Sorlie PD, Stein J, Turan TN, Virani SS, Wong ND, Woo D, Turner MB. Heart disease and stroke statistics--2013 update: a report from the American Heart Association. Circulation. 2013; 127:e6–e245. [PubMed: 23239837]

Gough MJ. Preprocedural imaging strategies in symptomatic carotid artery stenosis. J Vasc Surg. 2011; 54:1215–1218. [PubMed: 21871773]

Grønholdt ML, Wiebe BM, Laursen H, Nielsen TG, Schroeder TV, Sillesen H. Lipid-rich carotid artery plaques appear echolucent on ultrasound B-mode images and may be associated with intraplaque haemorrhage. Eur J Vasc Endovasc Surg. 1997; 14:439–45. [PubMed: 9467517]

Grønholdt MLM, Nordestgaard BG, Bentzon J, Wiebe BM, Zhou J, Falk E, Sillesen H. Macrophages are associated with lipid-rich carotid artery plaques, echolucency on B-mode imaging, and elevated plasma lipid levels. J Vasc Surg. 2002; 35:137–45. [PubMed: 11802145]

Halliday A, Harrison M, Hayter E, Kong X, Mansfield A, Marro J, Pan H, Peto R, Potter J, Rahimi K, Rau A, Robertson S, Streifler J, Thomas D. 10-year stroke prevention after successful carotid endarterectomy for asymptomatic stenosis (ACST-1): a multicentre randomised trial. Lancet. 2010; 376:1074–84. [PubMed: 20870099]

Jaguszewski M, Klingenberg R, Landmesser U. Intracoronary Near-Infrared Spectroscopy (NIRS) Imaging for Detection of Lipid Content of Coronary Plaques: Current Experience and Future Perspectives. Curr Cardiovasc Imaging Rep. 2013; 6:426–430. [PubMed: 24098825]

Kardoulas DG, Katsamouris AN, Gallis PT, Philippides TP, Anagnostakos NK, Gorgoyannis DS, Gourtsoyannis NC. Ultrasonographic and histologic characteristics of symptom-free and symptomatic carotid plaque. Cardiovasc Surg. 1996; 4:580–90. [PubMed: 8909814]

Mauldin FW, Zhu HT, Behler RH, Nichols TC, Gallippi CM. Robust principal component analysis and clustering methods for automated classification of tissue response to ARFI excitation. Ultrasound Med Biol. 2008; 34:309–325. [PubMed: 17913334]

Moody AR, Murphy RE, Morgan PS, Martel AL, Delay GS, Allder S, MacSweeney ST, Tennant WG, Gladman J, Lowe J, Hunt BJ. Characterization of complicated carotid plaque with magnetic resonance direct thrombus imaging in patients with cerebral ischemia. Circulation. 2003; 107:3047–52. [PubMed: 12796133]

Moreno PR. Vulnerable plaque: definition, diagnosis, and treatment. Cardiol Clin. 2010; 28:1–30. [PubMed: 19962047]

Mughal MM, Khan MK, DeMarco JK, Majid A, Shamoun F, Abela GS. Symptomatic and asymptomatic carotid artery plaque. Expert Rev Cardiovasc Ther. 2011; 9:1315–30. [PubMed: 21985544]

Naim C, Cloutier G, Mercure E, Destrempes F, Qin Z, El-Abyad W, Lanthier S, Giroux MF, Soulez G. Characterisation of carotid plaques with ultrasound elastography: feasibility and correlation with high-resolution magnetic resonance imaging. Eur Radiol. 2013; 23:2030–41. [PubMed: 23417249]

Newby AC, George SJ, Ismail Y, Johnson JL, Sala-Newby GB, Thomas AC. Vulnerable atherosclerotic plaque metalloproteinases and foam cell phenotypes. Thromb Haemost. 2009; 101:1006–11. [PubMed: 19492140]

Nightingale KR, Soo MS, Nightingale R, Trahey GE. Acoustic radiation force impulse imaging: In vivo demonstration of clinical feasibility. Ultrasound Med Biol. 2002; 28:227–235. [PubMed: 11937286]

Pinton GF, Dahl JJ, Trahey GE. Rapid tracking of small displacements with ultrasound. IEEE Trans Ultrason Ferroelectr Freq Control. 2006; 53:1103–1117. [PubMed: 16846143]

Pislaru C, Kantor B, Kinnick RR, Anderson JL, Aubry MC, Urban MW, Fatemi M, Greenleaf JF. In vivo vibroacoustography of large peripheral arteries. Invest Radiol. 2008; 43:243–252. [PubMed: 18340248]

Redgrave JN, Gallagher P, Lovett JK, Rothwell PM. Critical cap thickness and rupture in symptomatic carotid plaques: the oxford plaque study. Stroke. 2008; 39:1722–9. [PubMed: 18403733]

Redgrave JN, Lovett JK, Gallagher PJ, Rothwell PM. Histological assessment of 526 symptomatic carotid plaques in relation to the nature and timing of ischemic symptoms: the Oxford plaque study. Circulation. 2006; 113:2320–8. [PubMed: 16651471]

Stary HC. Natural history and histological classification of atherosclerotic lesions: an update. Arter Thromb Vasc Biol. 2000; 20:1177–1178.

Ten Kate GL, Sijbrands EJ, Staub D, Coll B, ten Cate FJ, Feinstein SB, Schinkel AFL. Noninvasive Imaging of the Vulnerable Atherosclerotic Plaque. Curr Probl Cardiol. 2010; 35:556–591. [PubMed: 20974314]

Trahey GE, Palmeri ML, Bentley RC, Nightingale KR. Acoustic radiation force impulse imaging of the mechanical properties of arteries: In vivo and ex vivo results. Ultrasound Med Biol. 2004; 30:1163–1171. [PubMed: 15550320]

Vappou J, Luo J, Konofagou EE. Pulse wave imaging for noninvasive and quantitative measurement of arterial stiffness in vivo. Am J Hypertens. 2010; 23:393–8. [PubMed: 20094036]

Wasserman BA, Wityk RJ, Trout HH, Virmani R. Low-grade carotid stenosis: looking beyond the lumen with MRI. Stroke. 2005; 36:2504–13. [PubMed: 16239630]

Watanabe Y, Nagayama M, Suga T, Yoshida K, Yamagata S, Okumura A, Amoh Y, Nakashita S, Van Cauteren M, Dodo Y. Characterization of atherosclerotic plaque of carotid arteries with histopathological correlation: vascular wall MR imaging vs. color Doppler ultrasonography (US). J Magn Reson Imaging. 2008; 28:478–85. [PubMed: 18666148]

Wintermark M, Jawadi SS, Rapp JH, Tihan T, Tong E, Glidden DV, Abedin S, Schaeffer S, Acevedo-Bolton G, Boudignon B, Orwoll B, Pan X, Saloner D. High-resolution CT imaging of carotid artery atherosclerotic plaques. Am J Neuroradiol. 2008; 29:875–82. [PubMed: 18272562]

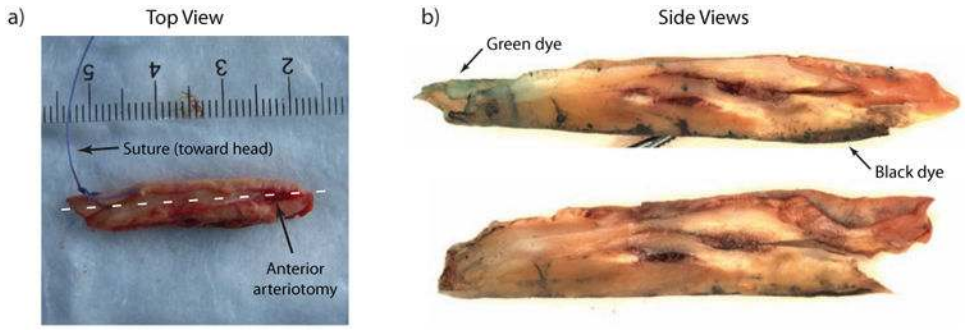

Figure 1.

Example of a sample preparation for histology. Panel (a) shows a top-view photograph of the raw sample from the common carotid of Patient A. The suture placed by the surgeon indicates proximal vs. distal end of the sample (with respect to the heart). The anterior surgical arteriotomy is evident on the top surface of the sample. To prepare samples for histology, the suture is removed and replaced with tissue marking dye and the sample is cut into two halves following the arteriotomy which approximates the ultrasound plane. Side views of the cut sample are shown in panel (b). Note the green and black tissue marking dyes in panel (b); green indicates suture position and black indicates the opposite side of the arteriotomy (i.e. the distal wall in the ultrasound image).

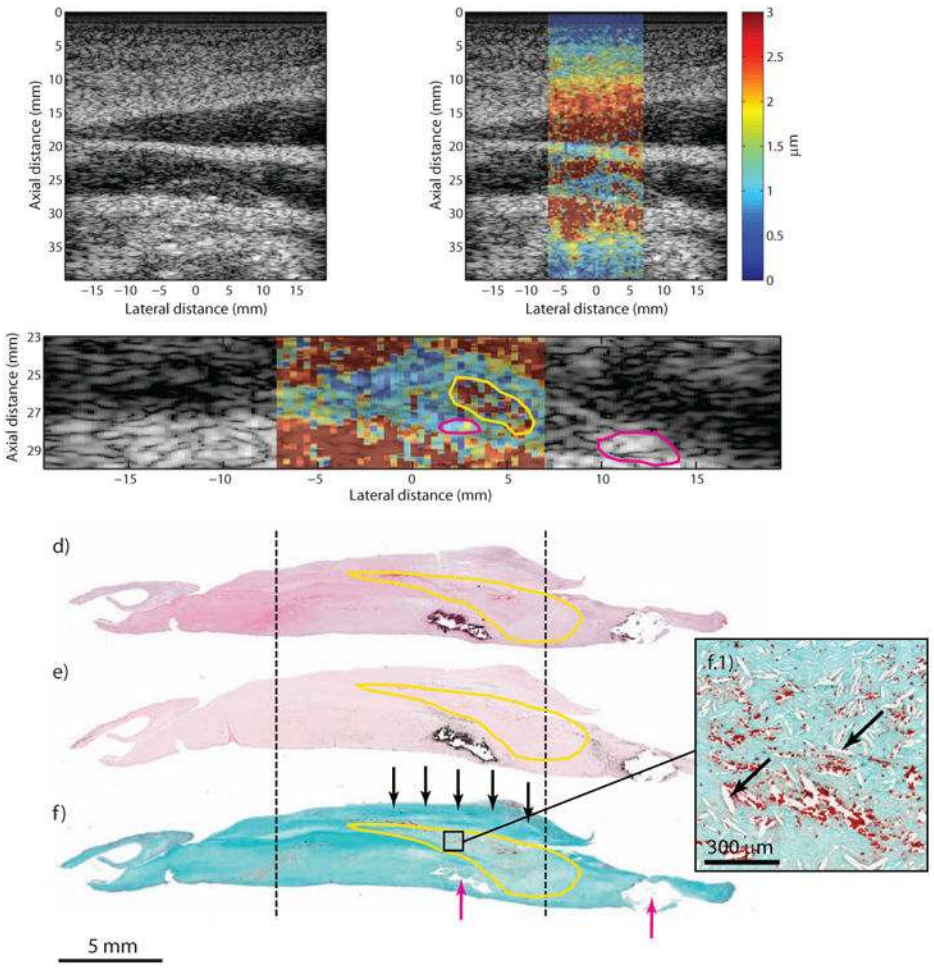

Figure 2.

Type Va plaque from the CCA of a 57 year-old, symptomatic male (patient A). B-mode imaging (a) shows an echolucent plaque with two echogenic foci separated by approximately 10 mm (white arrows). ARFI imaging (b) shows that the plaque is generally low-displacing except for a higher-displacing region located above the leftmost echogenic foci. ARFI magnification image is shown in (c); the solid white outline indicates extent of the plaque in the ultrasound image, the magenta outlines indicate the echogenic foci, and the yellow outline indicates the higher-displacing region. Histological staining with H&E (d), VK (e), and CME (f) shows a type Va plaque with a necrotic core and mild intra-plaque hemorrhage (yellow outline) and fibrous cap (f, black arrows). Two calcifications are seen at the bottom of the plaque (f, magenta arrows) separated by approximately 10 mm. Inset panel shows higher-magnification image of the necrotic/hemorrhagic region, which is denoted by cholesterol clefts (f.1, black arrows) and extravascular erythrocytes stained red (f.1). CCA, common carotid artery; CME, combined Masson's elastin; VK, Von Kossa.

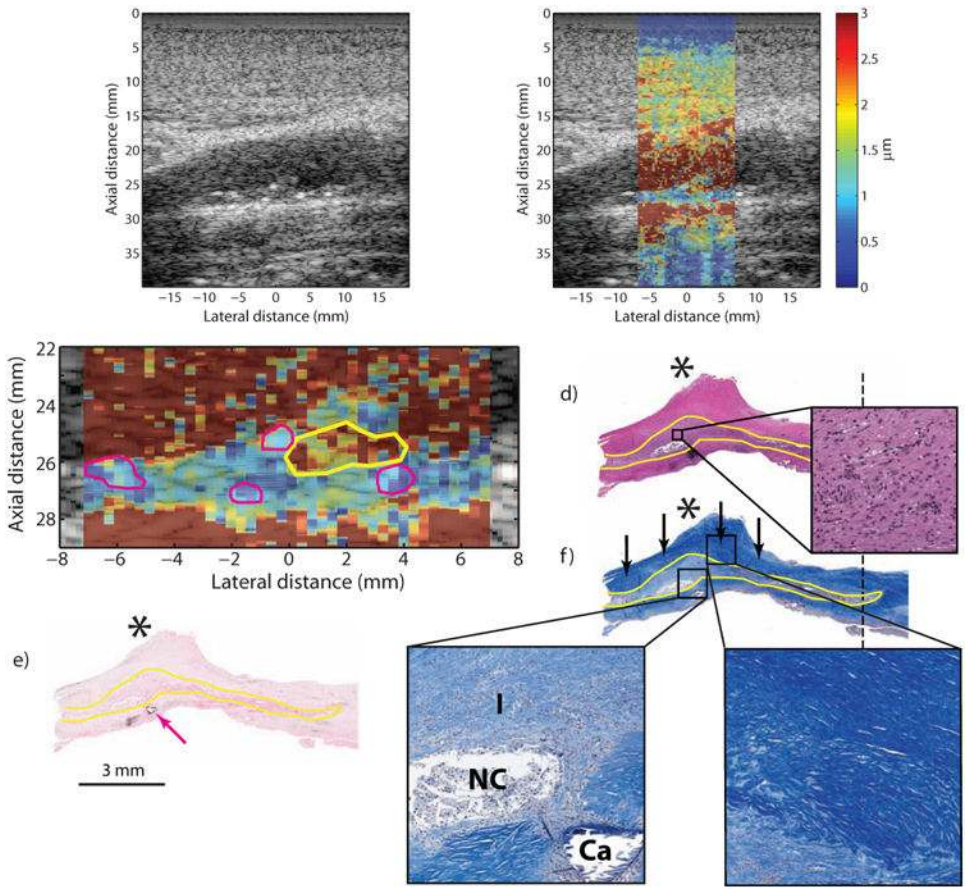

Figure 3.

Type Va plaque from the ICA of a 53 year-old, symptomatic female (patient B). B-mode image (a) shows a plaque on the distal wall with a protruding shoulder region (a, asterisk) and a number of small echogenic foci scattered throughout (white arrows). ARFI imaging (b) shows that the area beneath the shoulder region displaces farther than the rest of the plaque. ARFI magnification image is shown in (c); the solid white outline indicates extent of the plaque in the ultrasound image, the yellow outline indicates the higher displacing region, and magenta outlines indicate echogenic foci. Histological staining with H&E (d) and VK for calcium (e) shows a type Va plaque with a protruding shoulder region (d, asterisk) and small, submillimeter calcifications (e, magenta arrow). LMT staining for collagen shows abundant fibrosis in the shoulder region, indicated by the deep blue color (f, black arrows), which covers a cellular area with inflammation and a small, developing necrotic core. Inset panels show higher-magnification images of the cellular area just above the necrotic core (d. 1), the cellular area with the necrotic core (f.1) and the fibrous cap (f.2). The region of inflammation from histology is outlined in yellow. ICA, internal carotid artery; CCA, common carotid artery; LMT, Lillie's modified Masson's trichrome; VK, Von Kossa; I, inflammation; NC, necrotic core; CA, calcium.

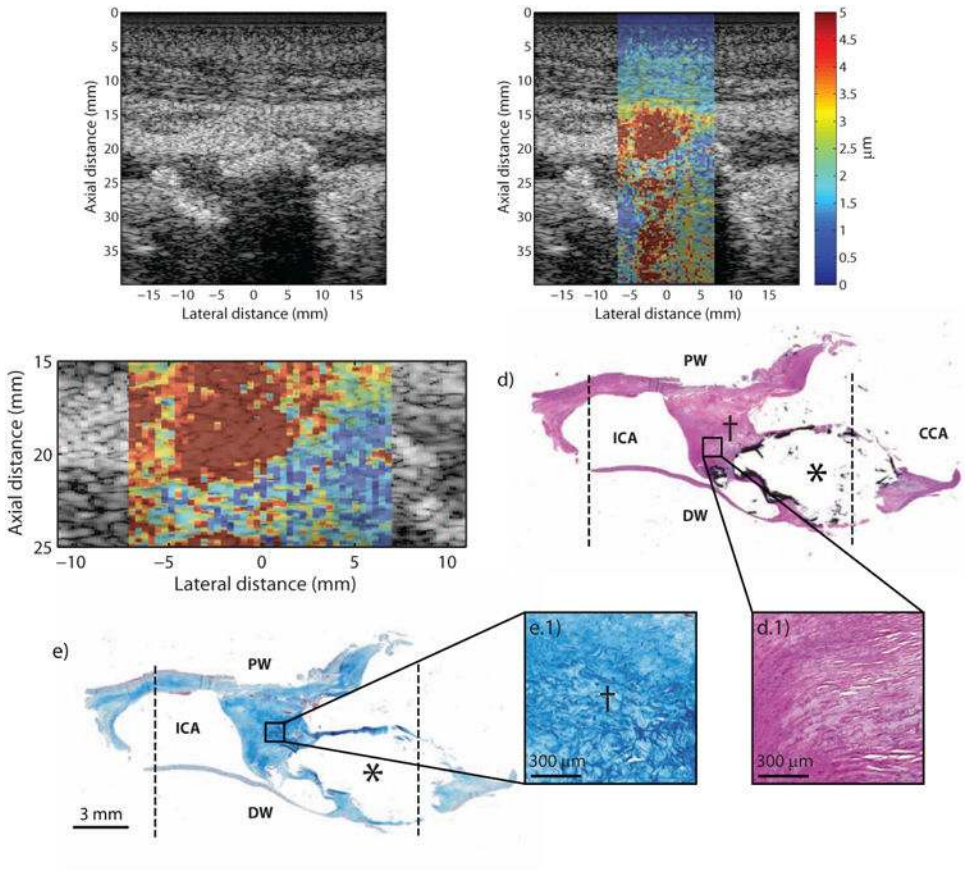

Figure 4.

Type Vb plaque from the ICA of a 72 year-old, asymptomatic male (patient C). B-mode image (a) shows a complicated lumen with a large area of shadowing (a, white arrows) from plaque in the distal wall. ARFI imaging (b) shows lower displacement in the area of the calcium deposit (asterisk) and higher displacements in the adjacent tissue connecting to the proximal wall (dagger). ARFI magnification image is shown in (c) with a white outline indicating the plaque that is above the shadowed region. Histological staining with H&E (d) and LMT for collagen (e) shows a large calcification (asterisk) indicated by the black stain. The dotted black lines indicate the extent of the ARFI FOV. Magnification insets shows that the tissue connecting the calcification to the proximal wall is comprised of loosely-packed (d.1) and disorganized (e.1) collagen fibers. ICA, internal carotid artery; CCA, common carotid artery; PW, proximal wall (with respect to transducer); DW, distal wall (with respect to transducer).

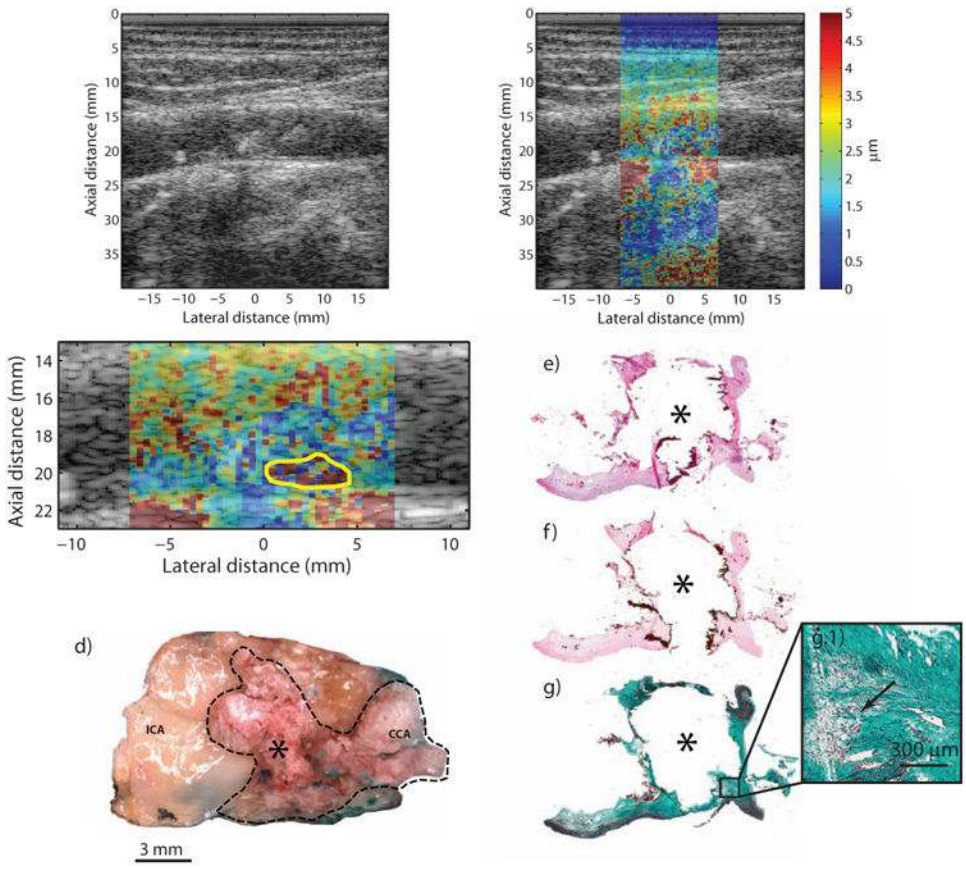

Figure 5.

Type Vb plaque from the ICA of a 65 year-old, asymptomatic male (patient D). B-mode image (a) shows a plaque extending significantly into the lumen with faint shadowing (white arrows) in the distal wall. ARFI imaging (b) shows a plaque with low displacement, except for a focal area of higher displacements located near the bottom of the plaque. ARFI magnification image is shown in (c); the solid white outline indicates extent of the plaque in the ultrasound image, and the yellow outline indicates the higher-displacing region. Gross macroscopic *en face* image of plaque (d) show areas of mineralization protruding into the lumen (dashed black outline). H&E, VK, and CME stains are shown in (e), (f), and (g), respectively. VK staining shows extensive calcification (asterisk). CME staining shows degraded collagen in areas surrounding the calcification (g.1, black arrow). Note that the lateral extent of the calcification was not captured in histology due to poor adhesion to the slide. ICA, internal carotid artery; CCA, common carotid artery.

Table 1

UNC stenosis grading scale

Class	Vel. Systolic (cm/sec)	Vel. Diastolic (cm/sec)	Category
1	< 160	< 80	0-39%
2	> 160	< 80	40-59%
3	> 160	80-109	Possibly > 60%
4	> 160	> 110	60-99%
5	0	0	Occluded
6*	See comment	See comment	See comment

*This grade is only given in special circumstances where further comments by the sonographer are necessary.

Table 2

Patient characteristics

Patient ID	A	B	C	D
Gender (M/F)	M	F	M	M
Age (years)	57	53	72	65
Stenosis grade	Class 6*	Class 4	Class 4	Class 4
Doppler-indicated systolic velocity (cm/s)	402	295	458	455
Doppler-indicated diastolic velocity (cm/s)	54	115	138	143
Arterial location of Doppler measurement	LCCA-Mid	RICA-Prox.	RICA-Prox.	LICA-Prox.
Symptomatic	Y	Y	N	N
Amaurosis fugax	N	Y	-	-
TIA	Y	Y	-	-
Completed stroke	N	N	-	-
ARFI focal depth (cm)	3.0	2.6	2.3	2.0
Peripheral vascular disease	N	Y	N	N
Diabetes mellitus	Y	Y	N	N
Hyperlipidemia	Y	Y	Y	Y
Hypertension	Y	Y	Y	Y
Smoking history	Y	Y	Y	Y

*Due to stenosis in CCA, sonographer noted that velocities in ICA may underestimate grade of ICA stenosis.

TIA = transient ischemic attack
ARFI = acoustic radiation force impulse
RICA = right internal carotid artery
LICA = left internal carotid artery
LCCA = left common carotid artery

Table 3

Histological stain guide

Stain	Feature	Color
Hematoxylin and Eosin (H&E)	Nuclei	Dark blue
	Cytoplasm/extracellular matrix	Pink
	Erythrocytes	Red
Von Kossa (VK)	Calcium	Black
	Cytoplasm/extracellular matrix	Pink
Combined Masson's Elastin (CME)	Elastin fibers, nuclei	Black
	Collagen	Green
	Erythrocytes, thrombus, cytoplasm, muscle fibers, keratin	Red
Lillie's Modified Masson's Elastin	Nuclei	Black
	Collagen	Blue
	Erythrocytes, thrombus, muscle fibers, fibrin	Red

Table 4
AHA classification system for atherosclerotic plaques

Type	Plaque composition
I	Isolated macrophage foam cells
II	Multiple foam cell layers formed, fatty streak
III	Pre-atheroma with isolated extracellular lipid pools
IV	Atheroma with confluent extracellular lipid core
Va	Fibroatheroma surrounded by fibromuscular tissue layers with lipid or necrotic core (sometimes classified as simply type V)
Vb	Calcification predominates (sometimes classified as type VII)
Vc	Fibrous tissue changes predominate, absent/minimal lipid core (sometimes classified as type VIII)
VI	Fissured, ulcerated, hemorrhagic, thrombotic lesion